A new parallel plate shear cell for *in situ* real-space measurements of complex fluids under shear flow

Yu Ling Wu
Soft Condensed Matter, Debye Institute, Department of Physics and Astronomy, Faculty of Science, Utrecht University, P.O. Box 80000, 3508 TA Utrecht, The Netherlands

Joost H. J. Brand,[a] Josephus L. A. van Gemert, and Jaap Verkerk
Scientific Instrumentation, Faculty of Science, Utrecht University, P.O. Box 80004, 3508 TA Utrecht, The Netherlands

Hans Wisman, Alfons van Blaaderen, and Arnout Imhof[b]
Soft Condensed Matter, Debye Institute, Department of Physics and Astronomy, Faculty of Science, Utrecht University, P.O. Box 80000, 3508 TA Utrecht, The Netherlands

(Received 30 May 2007; accepted 12 September 2007; published online 3 October 2007)

We developed and tested a parallel plate shear cell that can be mounted on top of an inverted microscope to perform confocal real-space measurements on complex fluids under shear. To follow structural changes in time, a plane of zero velocity is created by letting the plates move in opposite directions. The location of this plane is varied by changing the relative velocities of the plates. The gap width is variable between 20 and 200 μm with parallelism better than 1 μm. Such a small gap width enables us to examine the total sample thickness using high numerical aperture objective lenses. The achieved shear rates cover the range of $0.02-10^3$ s^{-1}. This shear cell can apply an oscillatory shear with adjustable amplitude and frequency. The maximum travel of each plate equals 1 cm, so that strains up to 500 can be applied. For most complex fluids, an oscillatory shear with such a large amplitude can be regarded as a continuous shear. We measured the flow profile of a suspension of silica colloids in this shear cell. It was linear except for a small deviation caused by sedimentation. To demonstrate the excellent performance and capabilities of this new setup we examined shear induced crystallization and melting of concentrated suspensions of 1 μm diameter silica colloids. © *2007 American Institute of Physics.* [DOI: 10.1063/1.2794226]

I. INTRODUCTION

Complex fluids exhibit a rich phase behavior under undisturbed conditions. Owing to their softness, applying an external field, such as a shear flow, makes their behavior even more interesting.[1] Shear may, for example, change the location of phase boundaries, induce both crystallization and melting, or even produce entirely new microstructures.[2–7] A system under shear can also separate into phases with different viscosities leading to shear banding. Shear can also promote a specific orientation: polymers stretch in the flow direction[8] and colloidal particles tend to align in the flow direction.[9,10] Liquid crystalline systems can undergo an isotropic to nematic transition under shear.[11–13]

Controlled application of shear stress or strain as in a rheometer allows one to measure bulk material properties such as yield stress, elasticity, and viscosity.[14] They come in different geometries, all with their own strengths and limitations. The Couette cell is widely used for continuous or oscillatory shear measurements. The parallel plate and the cone-plate geometries have the advantage that both the shear rate and shear strain are uniform throughout the cell. With a parallel plate shear cell, one can only apply an oscillatory shear, but if the travel is long enough the shear can be regarded as continuous. For determining the influence of the shear rate on a given system, the parallel rotating disk shear cell is a good choice. In this geometry, both the shear rate and shear strain increase in the radial direction.

While material properties such as viscoelasticity are useful to know, it is difficult to relate them to the materials microstructure and structural changes under shear. Therefore, shear cells have been designed such that it can examine the sample's microstructure under shear. At first, they were mostly combined with scattering techniques such as small-angle x-ray scattering (SAXS),[15–19] small-angle neutron scattering (SANS),[20–22] and small-angle light scattering (SALS),[23–27] which yield information over a large sample volume. In many cases, structural data are needed on a more local level than scattering can provide, or the flow itself becomes nonuniform. In addition, without a good model of what is happening with the structure, scattering data are hard to interpret. Thus, shear cells have been combined with optical microscopy in recent years.[22,28–41] As not every type of shear cell is amenable to microscopic inspection, these cells are usually of the cone-plate or parallel plate type.

An important step forward in the ability to quantitatively investigate complex fluids was the development of confocal scanning laser microscopy (CSLM).[42] This technique enables

[a]Electronic mail: j.h.j.brand@phys.uu.nl; URL: www.science.uu.nl/instrumentatie
[b]Electronic mail: a.imhof@phys.uu.nl; URL: www.colloid.nl

one to reveal the three-dimensional (3D) structure by examining samples slice by slice at submicrometer resolution.[43–47] However, if structural changes are to be studied under shear, one must prevent objects in such a slice from moving through the field of view too fast. One option is to momentarily interrupt the flow for taking images,[38,41] but this is possible only in slow systems. Moreover, particle tracking becomes very difficult. A good, but technically more demanding, alternative is to create a zero-velocity plane (ZVP) by moving the two parts of the shear geometry in opposite directions. This concept was introduced by Taylor in his study of droplet breakup[48] and has since been applied in several shear cells of different design.[34–36] These cells cannot, however, be used in combination with confocal microscopy using high numerical aperture (NA) oil immersion objectives.

The study of sheared complex fluids at submicrometer resolution places extreme demands on the stability of the shear cell as well as on the uniformity of the flow created by it. Recently, a parallel plate shear cell with a ZVP was described[32] that is accessible with CSLM, but it lacks the mechanical stability needed to stably image colloidal objects. A cone plate shear cell with a ZVP was constructed that does achieve the required stability.[29] Its limitations are that the gap width exceeds the working distance of high NA objectives, so that only the lower part of the gap can be observed. Moreover, the cone and plate are too heavy to allow oscillatory shear experiments at any but the lowest frequencies.

Therefore, we developed a new high precision parallel plate shear cell with a very stable ZVP. This cell can be mounted on top of an inverted confocal microscope; the sample cell is optically accessed through the bottom glass plate. To make optimal use of the resolution of the confocal microscope in imaging individual colloidal particles, high numerical aperture oil immersion objective lenses are used. These objectives have a working distance of around 100 μm, assuming that imaging is done through a No. 1 microscopy glass slide of 160 μm thickness. So, even when the bottom glass plate is as thin as 160 μm, only the lower 100 μm of a sample can be examined. Because complex flow profiles may occur in sheared complex fluids, we wanted to be able to view the complete gap. We, thus, chose a gap that is adjustable from 20 to 200 μm. With such a narrow gap and using micron-sized particles, a variation in the position of the plates of even a few micrometers becomes significant. The cell was therefore designed to be very stable, and the motion of the plates was made parallel to high accuracy. As we use small sample volumes, a vapor lock was included to limit evaporation. This shear cell can apply shear rates in the range of $0.01-10^3$ s^{-1}, which is the useful range for most complex fluids. The amplitude of the oscillatory shear can reach up to 1 cm, in which limit is large enough to be regarded as a continuous shear for most systems. Furthermore, a transparent window is made in the top plate to allow for light scattering experiments. Finally, we chose a modular design. The glass plates that are in contact with the sample are attached to cassettes that are placed in translation stages moved by piezomotors. The glass plates are exchangeable, simplifying cleaning and making it possible to examine, for example, the influence of wetting properties or surface patterning by using specially prepared plates. New cassettes can also be designed for specific experiments, e.g., to apply an electric field or to measure forces during shearing. Limitations of our shear cell are that it is not temperature controlled. The cell must also remain horizontal, making it difficult to perform SAXS or SANS measurements.

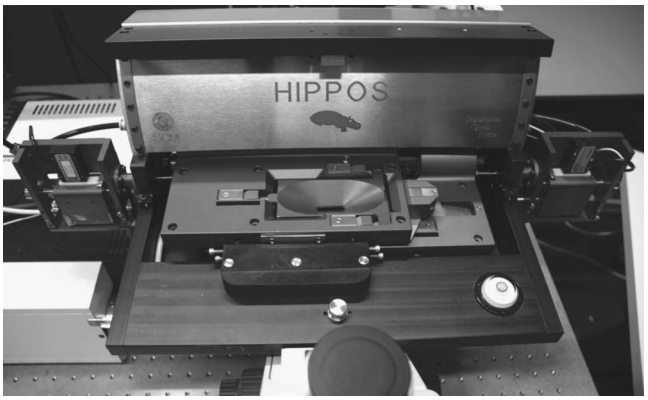

FIG. 1. Photograph of the parallel plate shear cell placed on top of an inverted confocal microscope.

II. SHEAR CELL CONSTRUCTION

A. Layout of the shear cell

Samples are sheared between two glass plates that are attached to two cassettes. The bottom translation stage contains the removable bottom cassette with the bottom glass plate, usually a microscopy coverslip. The top translation stage has a similar cassette for holding a top glass microscope slide. When the stages are in center position, first the bottom and then the top cassette can be inserted. The main frame supports both translation stages and their guide rods. Attached to the sides are two independently mounted motors that separately drive the top and bottom stages via connecting rods. Both the translation stages and the motor stages are borne by air bearings. Figure 1 shows the shear cell as placed on top of an inverted confocal microscope. Figure 2

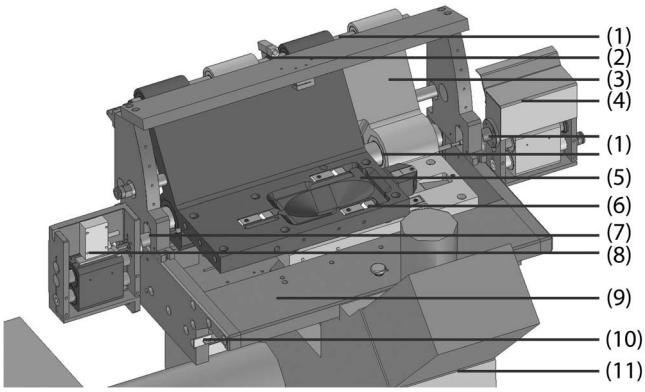

FIG. 2. Schematic representation of the shear cell as placed on top of an inverted confocal scanning laser microscope. (1) Air bearing, (2) secondary guide rod, (3) bottom translation stage, (4) motor bottom stage, (5) top cassette, (6) tilt and gap adjustments, (7) main guide rod, (8) motor top stage, (9) main frame, (10) cross adjustment lever, and (11) confocal microscope.

TABLE I. Achieved range of various parameters of our high precision parallel plate oscillating shear cell.

Gap width	20–200 μm
Cell size	15 mm × 30 mm × gap width
Cell volume	9–90 μl
Speed per plate	2.5 μm/s–10 mm/s
Shear rate	$0.02–10^3$ s^{-1}
Maximum travel of each plate	10 mm

is a schematic representation in which all components are indicated.

The glass plates need to be exactly parallel to the axis of motion, and the gap width has to be adjustable. Each cassette is therefore supported by three bearing balls that can be adjusted individually or in combination, to minimize tilt or to adjust the gap, respectively. The whole shear cell rests on the microscope frame and is therefore nearly parallel to the focal plane of the microscope. Over the limited plane of view (at most several hundred micrometers), any residual misalignment is negligible and does not have to be made adjustable.

With a cross adjustment lever, the pair of stages can also be shifted a few millimeters perpendicular to the translation axis. This is useful for finding a suitable area for imaging.

B. Design of a high precision shear cell

Creating a shear cell with a high precision and a steady zero-velocity plane requires a solid mechanical design of the stages and the cassettes, a proper alignment of the glass plates, a constant gap, and a well-designed velocity control loop. At the high precision required, no stick-slip or play can be tolerated neither in the driving system nor in the linear guides. Any force or other effect that is not constant will cause a noticeable effect on the stages. All these effects have to be mapped in advance. By a consequent application of design rules for high precision equipment, the effects cannot be eliminated but their effect in the imaging volume can be reduced as much as possible to achieve stable imaging of samples under shear. Table I lists the achieved range of various parameters of this cell.

C. Design of the stages

One of the requirements of the shear cell is that it has a steady zero-velocity plane. The microscope on which this cell is used has a resolution of 0.2 μm in the *xy* plane, i.e., in the plane perpendicular to the optical axis of an inverted microscope. To make optimal use of the resolution of the microscope, the linearity of the shear cell and its controller has to be within 0.05 μm. This is a very high goal if the production errors of the different parts are typically around 10 μm. Even the grinded rods have been made with a precision of 1 μm. This extreme relation between production tolerances and the required precision of the cell makes the fact that the design has to have intrinsic accuracy. In the design process, all the process forces (desired or undesired) have been mapped. The main design effort was to assure that the forces are applied in places where they cause minimal deflections in the imaging area. Calculating the remaining deflections is a time-consuming process that depends a lot on the presumptions made. So for the most crucial parts, tests have been made to assure in an early stage that the required accuracy could be achieved.

To eliminate displacements of the shear cell relative to the microscope (that is, between sample and objective), which would lead to a disturbance of the images, we chose to place the shear cell on top of the microscope. Therefore, the shear cell has to be relatively lightweight (a weight of 12 kg is achieved) and a compact construction with high stiffness is needed. To estimate the required stiffness, an inventory of all the disturbing forces that are exerted on the frame and the stages has been made. This shows that the largest disturbance is caused by the "cg shift," i.e., by the moving of the center of gravity of each stage (roughly 3 kg per stage) over the full travel of 15 mm.

Bushings have been chosen as bearings as they constrain four degrees of freedom within a very compact space. A stage such as this can be guided along a round main guide rod, fixing four degrees of freedom. It needs a second parallel guidance to fix the fifth degree of freedom: a rotation around the main guide rod. The sixth degree is the required shear motion.

The required parallelism of both guide rods is higher than what our production facilities provide. The forces of the shearing motion make that even harder. A stiffness of 10^7 N/m has been achieved within the stages (and not in the frame) by making them out of one piece. In this design, it is the stages that hold both rods parallel and not the external frame. The achieved stiffness in the stages makes it impossible to achieve nanometer precision along the whole stage. Warp and deflections do occur, but by careful design, the precision is at its maximum where it is needed: in the focus of the microscope. The external frame is there to hold the cell on the microscope and to protect it. This setup has been developed according to the following specifications and requirements:

- Both stages are guided by the same set of parallel guide rods. This ensures maximum parallel movement of the two stages: If the cell tilts by the cg shift, both stages tilt but remain parallel.
- The stages have an angled design. The angle is a design parameter that has been adjusted to place the center of gravity of the stages very close to the vertical plane of the main guide rod: this reduces the bending forces on the secondary guide rod to nearly zero.
- The stages provide the required stiffness of 10^7 N/m. The main frame is there only to position the cell on the microscope.
- The secondary rod is held in bushing bearings as they are very compact. Undesired effects of the overconstrainment have been eliminated by constraining the secondary guide rod only in the single direction needed: tangential to the rotation of the main rod.
- By overconstraining the secondary guide rod, it has become self-aligning with the main guide rod. (Fixing the screws of the secondary bushings while they are "on air" and with moving stages aligns them with the axis of motion, defined by the main axis.)

- The air bearings of the secondary guide rod are mounted in the plane normal to the (angled) back plane of the stages. Production tolerances on this mounting plane result only in stresses within the plane and give minimal displacement errors (stresses normal to the plain would cause warp and deflections).
- By giving the secondary guide rod (13 mm) a lower stiffness than the main guide rod (25 mm), extra stress reduction $(13/25)^3$ is obtained in the stages
- The shear gap is at the same height as the center of the main guide rod to reduce Abbe errors.
- The use of porous air bearings (New Way) evens out production inaccuracies (of roughly 1 μm) of the guide rods over a relatively large area. The bearings are self-aligning.
- The centers of mass of the stages are closely adjacent to the outside of the main guide rod so that the motor rods can be mounted exactly in the center of mass. Doing so, acceleration and deceleration forces only cause minimal dynamic errors.
- The position measurement of both stages is performed with an optical pickup unit. These units are placed very close to the center of mass of the stages and as close as possible to the focus of the microscope.
- Adjustments to the above rules have intentionally been made with some offset to avoid cycling of forces through zero. For example, the centers of gravity of the stages lie slightly to one side of the axis of the main guide rod so that the secondary guide rod always remains slightly loaded in one direction.

D. The motor stages

Piezostepper motors (Nanomotion, HR2) were chosen for their wide dynamic range, infinite stroke, and high precision. In addition to the driving force, these motors exert a force normal to the axis of motion. To avoid deformation of the translation stages, separate motor mounts have been designed. These mounts have two additional functions: (1) To supply air to the translation stage via a special passage through one of the air bearings so that undesired stresses caused by bending of air hoses are avoided. A chamber in the modified bearing transmits the air from the hollow supply axis to the motor mount and translation stage. (2) Modular function separation: optimizations in the actuate and control loop can be done without having to modify the whole shear cell.

E. Cassette design

Both stages have a cassette to which microscopy glass slides are attached. The glass slides between which a sample is sheared need to be attached to the cassette with an extreme flatness on the sample side. For every experiment, new glass slides are glued onto the cassettes. Between the glass and cassette, a soft paper mask is applied soaked with an epoxy glue. The soft paper is an easy way of applying glue where it is needed and it functions as a bed of tiny springs for the flexible glass slides. During curing of the glue a $\lambda/20$ optical flat is pressed on the glass slide, functioning as a flatness reference. An interference pattern appears and the shape of this pattern is an instantaneous check to see whether a high flatness is obtained. The thickness of the paper/glue layer is found to be 250 ± 20 μm.

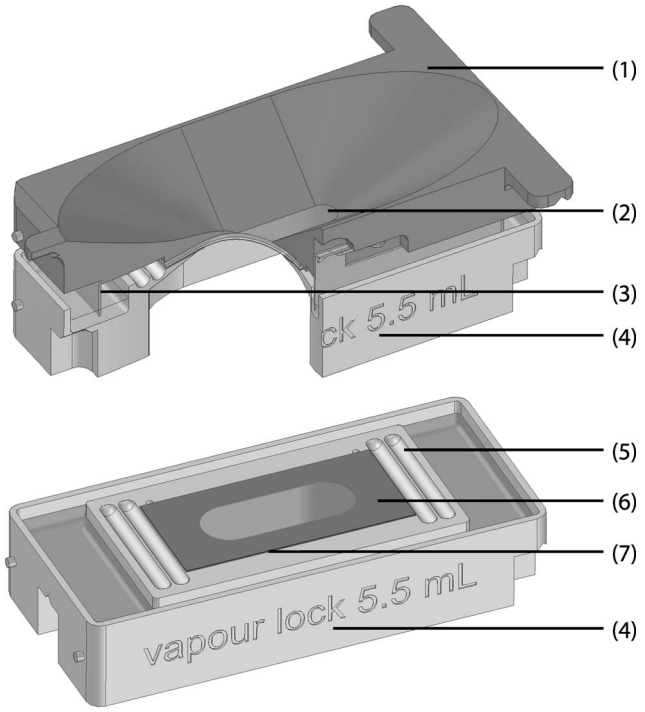

FIG. 3. The bottom and top cassette. (1) Top cassette ($10\times2.5\times1.6$ cm^3), (2) transparant window that allows for light scattering, (3) metal ring to seal the sample cell, (4) bottom cassette ($10\times2.5\times1.6$ cm^3) with a gap to fill with solvent, (5) solvent for vapor pressure, (6) microscope glass slide, and (7) paper glue mask.

To minimize evaporation, a vapor barrier is made consisting of a rectangular metal ring hanging in a channel filled with solvent or inert liquid (see Fig. 3). Inside the thus sealed sample cell, there are two additional gullies to fill with the solvent and to collect spillover during shearing. The solvent maintains a constant vapor pressure that prevents the sample from drying out.

To test the parallelism of the two translation stages, a second set of cassettes was designed. Instead of microscopy glass slides, they each carry an optical flat. It is then possible to separate possible height deviations in contributions from (1) deviations in the movement of the stages and (2) unevenness of the glass slides.

F. Cassette alignment

To align the glass slides with the axis of motion, the cassettes have to be aligned one by one. Each cassette is supported by three bearing balls. In order to align a cassette, the height of each ball has to be separately adjustable. To set the desired gap width, the height of the three balls of the upper cassette has to be adjusted all by the same amount. A universal compact module has been developed that can combine an individual and a grouped adjustment (Fig. 4).

A lightweight and stiff construction to allow for a grouped adjustment is achieved by coupling the three modules of one cassette by a horizontal plate. The three modules for one cassette have been mounted in this single plate to

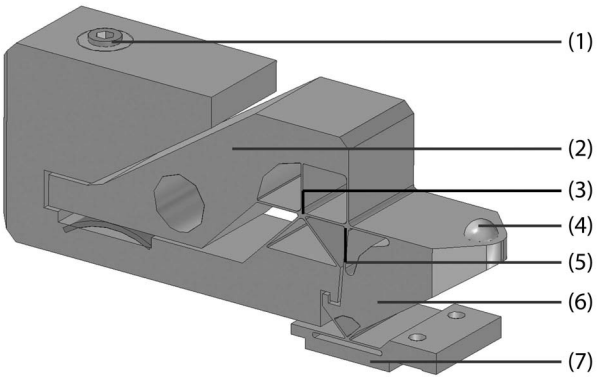

FIG. 4. Mechanism to adjust the height of the balls that support the cassettes. (1) Single point adjustment screw, (2) lever, (3) pivot of lever, (4) cassette support ball, (5) pivot of rocker, (6) rocker, and (7) grouped rocker adjustment.

couple the movements. A rocker converts the horizontal plate movement to the vertical ball movement. The hinge of this rocker is mounted on a lever that applies the individual adjustment. By doing so, both movements are added up to one ball lift. Only little space is available for the mechanism. High stiffness and relatively large deflections are therefore needed in the leaf spring hinges. A normal leaf spring has limited stiffness normal to its plane. Cross leaf hinges cannot be made in one step by wire electrical discharge machining (wire-EDM). The configuration as used here, referred to as "star leaf hinges," gives relatively large deflections and a high stiffness within a simple to produce geometry. The mechanism is free of stick-slip and play. It is also rigid enough to withstand the acceleration and shear forces encountered in typical experiments.

G. The control loop

The total travel of both stages is 10 mm. This is so large that capacitive position sensors cannot be used. To cover a range of shear rates relevant for complex fluids, the velocity of each stage has to range from 2.5 μm/s to 10 mm/s, with a maximum deviation from the desired speed of 2%. Linear tacho generators for this wide speed range are hard to find, so two LIP372 linear position encoders (Heidenhain) are used to obtain a position signal with a sufficiently high signal frequency at the lowest speed to avoid dither. A Galil DMC2040 controller is used to control the Nanomotion HR2 piezostepper motors. The controller is fast enough to handle the quadrature signal from the position encoders also at maximum speed.

The HR2 piezosteppers use two resonating ceramic fingers to step over a matching ceramic strip. A spring pushes the fingers against the strip. On one half of the electronic signal, the finger will push the stage in one direction. On the other half of the signal, the finger moves back. Moving backwards, the finger moves so fast that inertia of the stage and a limited friction make the finger break free from the strip. Depending on the shape of the signal, the stage is pushed in forward or backward direction. These motors have a very high positioning resolution. Yet, at speeds as low as a few μm/s, most piezostepper motors do not provide a smooth and constant speed behavior. The Nanomotion AB5 motor controller can add a subtle hammer function to the standard elliptical movement of the finger. This ensures that even at the smallest amplitude the stepper finger can break free from the strip and that a step is made. The measure and control loop as created for this shear cell has proven to work well over the whole speed range.

A graphical user interface has been made in which the user can control the shear settings. The speed of the plates, the velocity ratio with which the top and bottom plate move, and, thus, the height of the zero-velocity plane, amplitude, starting position along the velocity axis, and motion functions such as sawtooth or sinusoidal can be set. For alignment, the stages can be moved by slider controls in the interface, whereas for an experiment, a continuous oscillation function can be set.

III. OPERATION

The bottom glass plate is a standard microscopy No. 1 (thickness of 0.13–0.16 mm) glass slide of 24×50 mm^2. The top plate is a No. 5 (thickness of 0.5–0.6 mm) glass slide cut to 15×30 mm^2 (Menzel). The slides have to be attached to the cassette in such a way that fluctuations in height and, thus, in the gap width are minimal. The glass slides and cassettes are first thoroughly cleaned with ethanol giving special attention to removing dust particles. Then, one sheet of double-sheeted tissue (Kleenex hand towels code 6762, cut to size) is cut to size with a hole matching the cassette's window. It is then soaked in mixed two-component glue (Bison epoxy rapid) and placed on a cleaned glass slide. The glass slide and sticking tissue are together stuck on the accompanying cassette. The tissue is used to absorb height fluctuations that unremoved dust particles can otherwise induce. During the couple of hours needed for the glue to harden, an optical flat is placed on top of the glass slide. This is done to obtain highly flat glass plates. The optical flat has a surface roughness of $\lambda/20$, and this flatness is passed on to the glass slide.

Before filling the sample cell, the plates are aligned one by one. The z position is determined with the microscope in reflection mode, using the reflection of the 488 nm line of the argon laser. Whereas we use oil immersion objectives during experiments, we use an air objective ($63\times$; 0.7 NA, Leica) for alignment to avoid immersion oil on the bottom side of the top plate, which is the inside of the sample cell. The relative z position of the glass-air interface is calculated from a yz image, i.e., in the vorticity-gradient plane. An example of such an image is given in Fig. 5. The intensity of the reflection was summed over each horizontal line and the maximum was taken as the position of the interface. This does not necessarily coincide with the glass-air interface, but because only differences between the positions found at different lateral positions are of importance, this possible deviation can be disregarded. The accuracy of the position determination is about 0.1 μm. Each plate is then moved over its total travel of 1 cm, and the z position at the two ends is compared. If necessary, the tilt is adjusted with the adjustment screws. After exchanging the objective for an oil im-

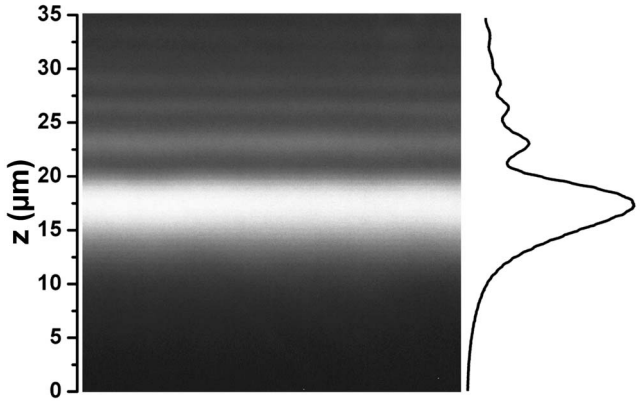

FIG. 5. (a) Example of the glass-air interface at the top side of the bottom plate imaged in reflection mode with a confocal microscope. From such an image, the position of the interface is determined by summing the intensities horizontally and determining the maximum. The most intense peak is taken as the glass-air interface. The less intense peaks are caused by interference.

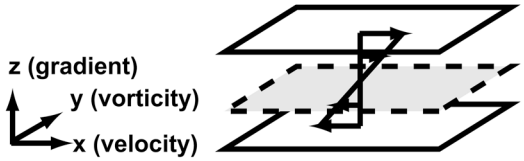

FIG. 6. Illustration defining our coordinate system. The optical axis of the microscope is along the vertical z axis. The zero-velocity plane (gray) is perpendicular to this axis and lies in the xy plane. Its vertical position can be set at any height. The velocity direction is along the x axis of the microscope. The vorticity direction is along the y axis and the gradient direction along the z axis.

mersion objective used for imaging in the experiments, the bottom cassette is loaded into the corresponding stage. The vapor barrier is then filled with 5.5 ml water, and a few droplets of the solvent are dropped into the vapor gully to bring the liquid in equilibrium with its vapor. This minimizes evaporation and, thus, a possible change in the concentration of the sample. Next, a few drops of the dispersion are set on the bottom plate. The volume of the dispersion has to be larger than the volume of the cell to avoid high capillary forces that could influence the flow behavior of the sample. Finally, the top cassette is slowly lowered on top of the dispersion and the desired gap width is set.

In the graphical user interface, the amplitude of the oscillation (A), the summed speed (v) of the plates, and the ratio of the speed of bottom (v_B) and top plate (v_T) are set. The gap width (d) connects these parameters to the shear rate, maximum strain, and height of the zero-velocity plane (z_{ZVP}) as given below. Table I summarizes the range of all settings. The shear rate $\dot{\gamma}$ is given by

$$\dot{\gamma} = \frac{v_T + v_B}{d}, \tag{1}$$

and the maximum strain γ_{max} by

$$\gamma_{max} = \frac{A_T + A_B}{d}. \tag{2}$$

The height of the ZVP is determined by the velocity ratio $r = v_B/v_T$ as follows:

$$z_{ZVP} = \frac{d}{1/r + 1}. \tag{3}$$

After the experiment, the glass plates can be detached by heating them to approximately 100 °C on a heating plate. The glue then becomes soft and the glass plates can easily be removed.

IV. EXPERIMENT

The shear cell was placed on top of an inverted Leica TCS-SP2 confocal scanning laser microscope. The 488 nm laser line of an argon laser was used for imaging. Scanning along the z axis was done using a piezofocusing drive (Physik Instrumente). This direction coincides with the gradient direction of the shear flow field. The velocity direction is along the x axis (see Fig. 6). All measurements were done in a room that was temperature controlled at 21±1 °C.

A. Determination of the alignment and motion of the plates

To create a steady flow profile, the plates have to be parallel to each other in the velocity direction. A roll around the x (velocity) direction does not influence the flow profile. It does influence the local shear rate though. To show that the plates are highly parallel, the z position of each plate was measured every 0.5 mm of the total lateral travel of 1 cm. With a 63×, 0.7 NA Leica air objective, the reflection of the 488 nm laser line was measured and the position of maximum intensity was taken as the glass-air interface.

Possible fluctuations in height may have two origins: (1) fluctuations in the z position of the stages and (2) a lack of flatness of the glass plates themselves. To distinguish between the two, the alignment measurements were performed both with a cassette containing an optical flat and with a (measurement) cassette with a No. 1 or 5 microscopy glass slide attached to it.

To show that the plates keep their parallelism while moving with the cell filled with a fluid, we measured the z position of the plates again after filling the shear cell. The fluids used were three silicone oils of different viscosities: 10, 50, and 1000 mPa s. All were obtained from Sigma Aldrich and used as received. A 63× Leica oil immersion objective with 1.4 NA was used for imaging.

Another condition needed to obtain a steady and uniform shear flow is an accurate movement of the plates in the velocity-vorticity plane. To monitor this movement, 1.2 μm diameter silica particles were adsorbed on the glass plates. While the plates were moving, xy images were taken with fixed time intervals. The two-dimensional (2D) cross-correlation functions of consecutive images were then calculated. The maximum of this function corresponds to the displacement of the plate. The accuracy of the displacement thus obtained is better than 0.1 μm. The cell was empty during this measurement.

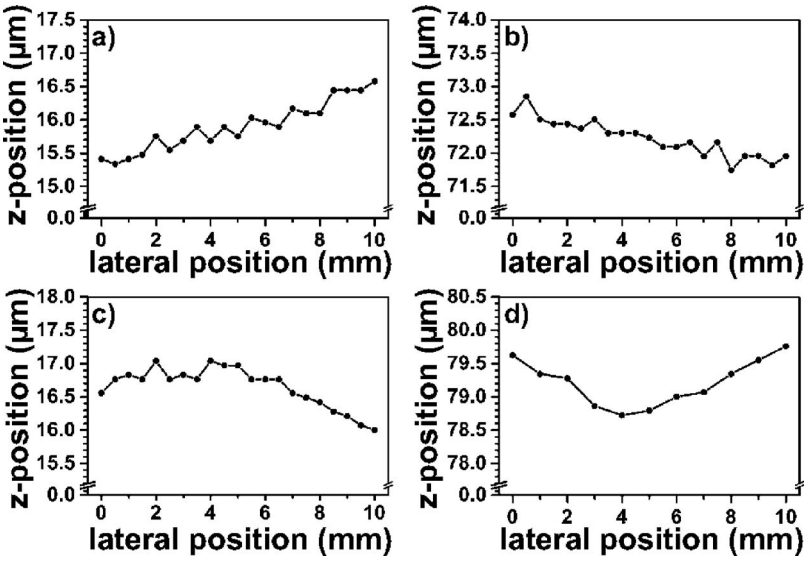

FIG. 7. Vertical position during a lateral displacement over a distance of 1 cm of (a) an optical flat in the bottom cassette, (b) an optical flat in the top cassette, (c) a No. 1 glass slide on the bottom cassette, and (d) a No. 5 glass slide on the top cassette. Fluctuations in z were only of the order of a micrometer.

B. Characterization of the flow profile

Flow profiles were measured using a dispersion of 1.2 μm diameter silica particles (at a volume fraction ϕ=0.22) in ethoxylated trimethylolpropane triacrylate [ETPTA, Aldrich, molecular weight (MW) of 428, viscosity $\approx$0.07 Pa s, used as received]. The particles were synthesized via a seeded Stöber growth.[49] A 0.4 μm diameter core of the particles was labeled with fluorescein isothiocyanate (FITC) using the method of van Blaaderen and Vrij.[50]

There are different methods to determine the flow profile. Probably, the most direct way is to take xz images with fixed time intervals. From the displacement of each particle, the average velocity at each height can be determined. A disadvantage of this method is that it can only be used when the velocity of the particles is low compared to the scan rate, because each particle has to be followed in time. A second method is to image particles in the xy plane. By cross-correlating consecutive images, the average displacement of the particles and, thus, the average velocity of that plane can be determined. Besides it only being applicable for low speeds, it has the disadvantage of being time consuming because it has to be done at several heights to obtain the complete flow profile.

Therefore, we used the quicker and easier method that Derks *et al.*[29] introduced to determine flow profiles. They took images at a slow scan rate in the velocity-gradient (xz) plane. Images are built up by scanning horizontal lines, i.e., along the x (velocity) direction. During a scan, the particles move. When a following line is scanned, the particles are displaced, which leads to an image in which the particles appear deformed. The degree of deformation depends on the local velocity of the dispersion. For a linear flow profile, the deformation becomes parabolic,

$$x(z) = \frac{\dot{\gamma} z}{\alpha}\left(\tfrac{1}{2}z - z_{\mathrm{ZVP}}\right), \tag{4}$$

where $x(z)$ is the position of a particle in a line scanned at height z, α is the scan rate in μm/s, and $\dot{\gamma}$ is the shear rate.

C. Observation of shear induced crystallization and melting of colloidal dispersions

To illustrate the performance of this shear cell and its usefulness in the field of soft condensed matter science, we describe an experiment showing shear induced crystallization and melting of a colloidal suspension. The suspension consisted of fluorescently labeled 1.2 μm diameter silica particles in ethoxylated trimethylolpropane triacrylate. The volume fraction was above the bulk crystallization volume fraction, which was around ϕ=0.50 for this system. To induce crystallization, a shear rate of 0.45 s^{-1} was applied. To melt the crystal afterwards, a shear rate of 2 s^{-1} was applied. The zero-velocity plane was set at 1/6th of the gap; with the gap used of 45 μm, this is at 7.5 μm from the bottom upwards.

V. RESULTS AND DISCUSSION

A. Determination of the alignment and motion of the plates

We performed a series of stringent tests to check the performance of the shear cell. First, the parallelism of only the stages was measured by monitoring the movement of the cassettes containing an optical flat. Figures 7(a) and 7(b) show that the bottom and top stages can be aligned such that over their total travel of 1 cm they only vary 1.3 μm (0.01%) and 1.2 μm (0.01%) in z, respectively.

Next, the optical flat was replaced by the glass slides that are used in a normal experiment. Fluctuations in the glass plates can be caused by stress built up when they are fixed to the cassettes, or by variations in their thickness. Figures 7(c) and 7(d) show, however, that these contributions are small and that the total variation in z stays within 1.1 μm. For our experiments, these small deviations are acceptable. Note that there was hardly any difference in the flatness of the bottom and the top plates, although the bottom plate is approximately four times as thin as the top one.

The plates must also stay parallel while moving with a fluid in between over a wide and relevant range of fluid viscosities. To test this, silicone oils with viscosities of 10,

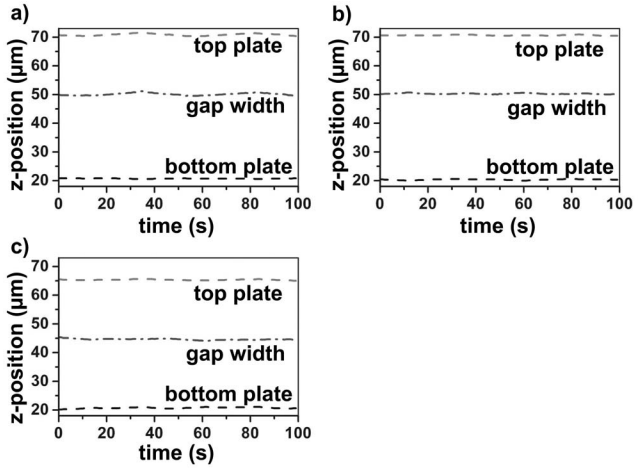

FIG. 8. Stability of the plates in z when the cell was filled with silicone oils with viscosities of (a) 10 mPa s, (b) 50 mPa s, and (c) 1000 mPa s. Both plates are moving with 250 μm/s in opposite directions. The change in z is only of the order of a micrometer while the travel of the plates is 6 mm.

50, and 1000 mPa s were chosen. Both plates travelled back and forth with an amplitude of $A_T=A_B=3$ mm at a speed of $v_T=v_B=250$ μm/s. The gap was about 50 μm. Figure 8 shows that the plates hardly fluctuated in z. They moved vertically over maximally 1–2 μm in z which equals to only 0.02%–0.03% of the travel. It corresponds to 2%–4% of the gap width though. The largest z fluctuations were measured when at the points where the plates changed direction. Problems arise when the sample volume is smaller than or equal to the volume of the cell so that a liquid meniscus forms. Then, capillary forces become so large that the two plates are pulled towards each other until a stationary gap width is reached. When the top plate is then lifted, the bottom plate raises over the same distance. The sample fluid should therefore always overfill the cell. To make this easier to do, we make the top plate smaller than the bottom plate.

Next, the movement in the velocity-vorticity plane must

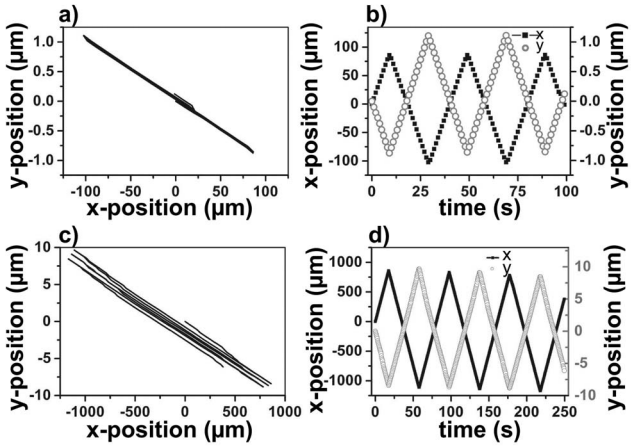

FIG. 9. The relative position of the top plate in the velocity-vorticity plane during an oscillatory movement. Panels (a) and (b) show data taken during a movement with $v_{top}=10$ μm/s and $A_{top}=100$ μm. Panels (c) and (d) show data taken during a movement with $v_{top}=50$ μm/s and $A_{top}=1$ mm. At a relatively high speed and a large amplitude, undesired movements in the vorticity direction were noted, but the effective error remained small.

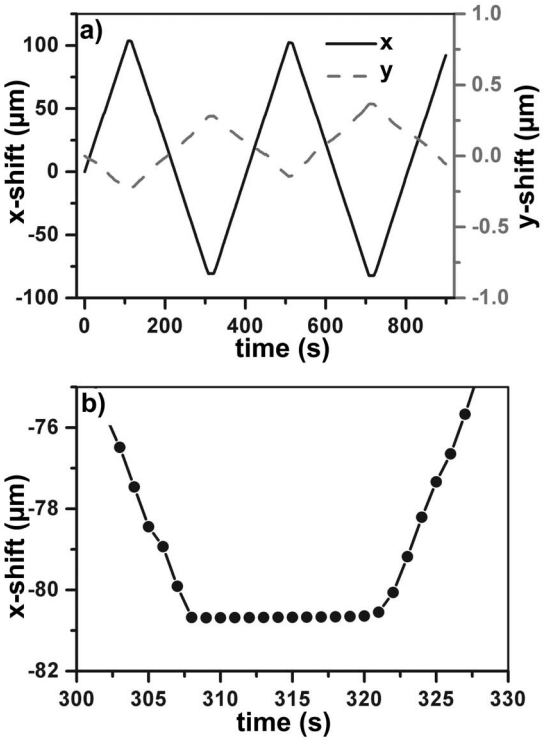

FIG. 10. The relative position of the top plate in the velocity-vorticity plane during an oscillatory movement ($v_{top}=1$ μm/s, $A_{top}=100$ μm). Panel (b) is a magnification of one of the turning points. At speeds as low as 1 μm/s, which is lower than the minimum speed for which the shear cell was designed, the top plate did not reverse instantly at the turning points. The period that the stage paused at the turning points was sometimes as long as 12 s.

be well defined: (1) there should be no drift in the velocity direction, meaning that after one oscillation the plates should return to their starting position, (2) the speed of the plates should be the same as or at least be proportional to the set speed, and (3) there should be no movement in the vorticity direction. To measure the movement, silica particles were adsorbed on the glass plates and their position was followed during an oscillation of the plates. The cell was empty during this experiment.

Figure 9 shows the position of the top plate during an oscillatory movement. First, the top plate was set to move with a speed of $v_T=10$ μm/s with an amplitude of $A_T=100$ μm [Figs. 9(a) and 9(b)]. The actual speed was determined by measuring the time needed to travel from a position just after one turning point to a position just before the

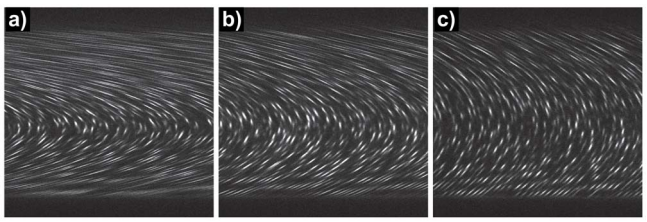

FIG. 11. Slowly scanned confocal microscopy images of the velocity-gradient plane of a colloidal dispersion sheared at shear rates of (a) 2.0 s^{-1}, (b) 1.0 s^{-1}, and (c) 0.5 s^{-1}. The applied ratio v_{bottom}/v_{top} was 0.5. The gap width was approximately 45 μm. The scan rate was $\alpha=5.8$ μm/s.

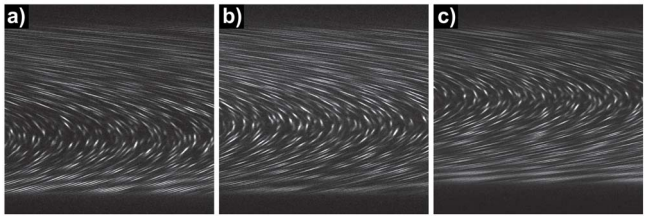

FIG. 12. Slowly scanned confocal microscopy images of the velocity-gradient plane of a colloidal dispersion sheared at a shear rate of 2 s^{-1}, but with different velocity ratios, v_{bottom}/v_{top}, (a) 0.33, (b) 0.5, and (c) 1.0. The gap width was approximately 45 μm. The scan rate was α=5.8 μm/s.

next turning point. The actual speed was 3% lower than the set speed. After each oscillation, the plate returned to very nearly its original position. Deviations were only minor and of the order of or smaller than the resolution of the microscope, which is 0.2 μm in the xy plane. It appeared that the axis of motion of the top plate and the x axis of the microscope make an angle of 0.6 °.

At higher speeds and larger amplitudes, the top plate still moved with only minor errors, as Figs. 9(c) and 9(d) and d show for a set speed of v_T=50 μm/s and an amplitude of A_T=1 mm. Although the plate no longer returned to its exact starting position after one oscillation, the error remained small. The actual speed was 2% lower than the set speed. Even at a speed of v_T=1 μm/s, which is lower than the minimum speed for which the shear cell was designed, the difference between the set and actual speed was only 3%, with the actual speed being lower than the set speed. However, at v_T=1 μm/s, the movement showed a delay at the turning points (Fig. 10). Instead of immediately changing direction at the maximum displacement, the stage stopped moving and started to move again after a certain time lag. A magnification of a turning point [Fig. 10(b)] shows that this time lag can be as long as 12 s. A short lag might also occur at high speeds, but if so, the delay occurring at a speed of 100 μm/s is smaller than the speed of our position detection which was 0.5 s.

The motion of the bottom plate showed a performance similar to that of the top plate. Again, the actual speed was slightly lower than the set speed: 3% at v_B=1 μm/s, 3% at v_B=10 μm/s, and 1% at v_B=50 μm/s. At v_B=1 μm/s, which lies outside the speed range for which this shear cell was designed, a time lag was again observed. The axis of motion of the bottom plate makes an angle of 0.7 ° with the x axis of the microscope. Thus, the axes of motion of the top and bottom plates are practically parallel, as they should.

B. Characterization of the flow profile

The sample for determining the flow profile was a dispersion of 1.2 μm diameter silica particles in ethoxylated trimethylolpropane triacrylate at ϕ=0.22. Images were taken in the velocity-gradient plane. Figure 11 shows the velocity-gradient plane of the dispersion sheared at different shear rates. During scanning of the image, the particles moved and, therefore, they appear deformed in the image, as given by Eq. (4). The degree of deformation depends on the local velocity. The zero-velocity plane is easily recognized at the top of the parabolas. From this deformation, the velocity at each height is determined using the method of Derks *et al.*[29] Because the ratio of the speeds of the bottom and top plate was fixed, the position of the zero-velocity plane did not change when the shear rate was varied. The apparent deformation of the particles is larger at higher shear rates. Figure 12 shows the velocity-gradient plane of the colloidal dispersion sheared at a fixed shear rate of 1.5 s^{-1} but with different ratios: v_B/v_T=0.33, 0.5, and 1.0.

Figure 13(c) shows the flow profiles thus obtained for the case that the bottom and top plate moved with a ratio of 1. The flow profile was nicely linear, as expected. Next, we measured the flow profile when the plates moved with a ratio of 0.33, 0.5, or 3 [see Figs. 13(a), 13(b), and 13(d)]. These flow profiles were slightly concave. Apparently, the shear rate at the bottom was slightly lower than at the top part of the sample. The zero-velocity plane was also located slightly lower than calculated from the set ratio [Eq. (3)]. After de-

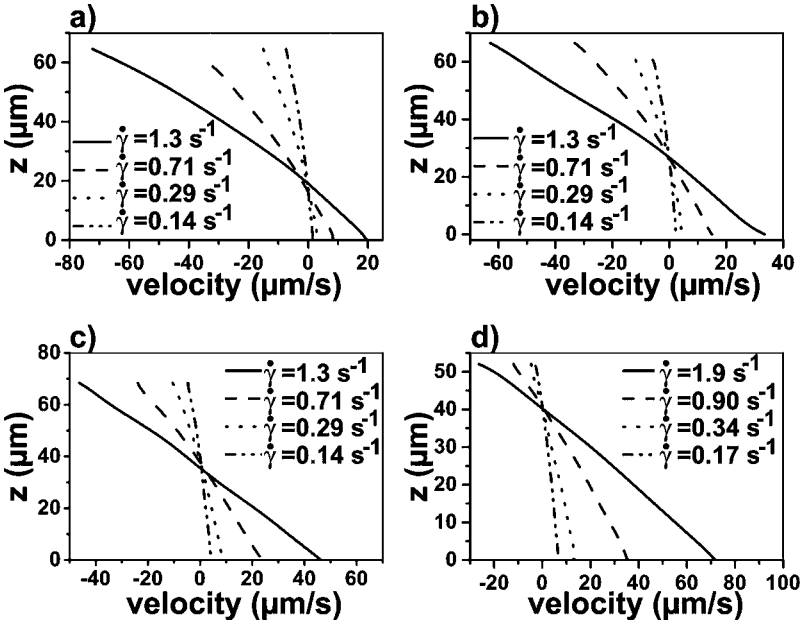

FIG. 13. Measured velocity vs height. The velocity ratio was (a) 0.33, (b) 0.5, (c) 1, or (d) 3. The different curves in each graph represent different shear rates. The curves cross at the position of the zero-velocity plane.

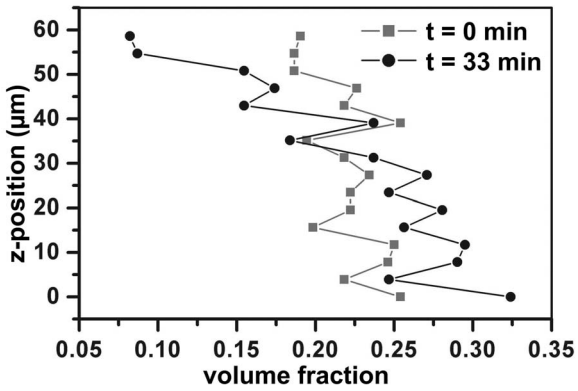

FIG. 14. In time, sedimentation of the particles caused the particle volume fraction near the bottom to increase.

termining the particle density as a function of height, we concluded that this deviation from linearity is due to sedimentation. Over time, the particles sediment (Fig. 14) leading to a locally higher viscosity which leads to a local decrease of the shear rate.

C. Observation of shear induced crystallization and melting of colloidal dispersions

At volume fractions above $\phi=0.50$, hard spherelike particles will order spontaneously. However, because the particles are relatively large and because the viscosity is high, this process may take hours. Before applying a shear flow, the particles were therefore randomly distributed. After application of a shear with shear rate $\dot{\gamma}=0.45\ s^{-1}$, the particles were seen to order in just a minute. Close-packed lines are oriented parallel to the flow direction. Figure 15 shows the evolution of the order in the zero-velocity plane. The sample was found to have crystallized throughout the cell with rows of particles aligned parallel with the velocity direction forming very large oriented crystals. When a high shear rate was applied ($\dot{\gamma}=2\ s^{-1}$), the sample slowly melted. This is shown in Fig. 16. In these experiments the zero-velocity plane makes it possible to track individual particles. We will report on the interesting melting and crystallization transitions under shear more quantitatively in a future publication.

VI. CONCLUSION

We have demonstrated a new parallel plate shear cell that enables microscopic observations of complex fluids us-

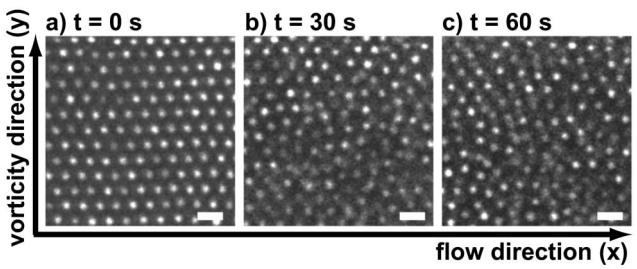

FIG. 16. Confocal micrographs of an initially crystalline dispersion of 1.2 μm diameter silica particles dispersed in ETPTA. At a shear rate of $\dot{\gamma}=2\ s^{-1}$, the average order of a dispersion decreased. The scale bars are 2 μm.

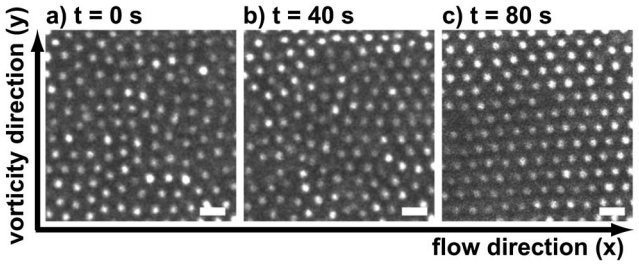

FIG. 15. Confocal micrographs of a dispersion of 1.2 μm diameter silica particles dispersed in ETPTA at $\phi\approx0.50$ during the application of a shear with $\dot{\gamma}=0.45\ s^{-1}$. Initially, the particles were not ordered but they gradually crystallized in time. The scale bars are 2 μm.

ing high NA objectives. The plates move in opposite direction creating a plane of zero velocity. It is possible to apply shear rates up to $10^2\ s^{-1}$. The plates only fluctuate 0.01% in height over a travel of 1 cm which is more than sufficient for creating a stable zero-velocity plane (ZVP) for imaging under shear flow. Even the bottom No. 1 glass plate was found to be stiff enough not to add any extra fluctuations in z position. Also, when the cell was filled with viscous silicone oils, the plates deviated less than 0.02% in z. The axis of motion was slightly rotated with respect to the x axis of the microscope, but apart from that, there was no significant deviation from linearity along the y axis. Flow profiles measured with dispersions of silica particles dispersed in a viscous medium were almost linear. A small deviation that is probably caused by sedimentation of the particles was noticeable.

An experiment of shear induced colloidal crystallization and shear induced melting observed in the ZVP illustrates the performance of the shear cell. It was possible to quantitatively follow the particles over a longer period of time.

ACKNOWLEDGMENT

This work is part of the research program of the "Stichting voor Fundamenteel Onderzoek der Materie (FOM)," which is financially supported by the "Nederlandse Organisatie voor Wetenschappelijk Onderzoek (NWO)."

[1] H. Löwen, J. Phys.: Condens. Matter **13**, R415 (2001).
[2] B. J. Ackerson and P. N. Pusey, Phys. Rev. Lett. **61**, 1033 (1988).
[3] B. J. Ackerson and N. A. Clark, Phys. Rev. Lett. **46**, 123 (1981).
[4] I. W. Hamley, J. A. Pople, C. Booth, Y.-W. Yang, and S. M. King, Langmuir **14**, 3182 (1998).
[5] Y. D. Yan, J. K. G. Dhont, C. Smits, and H. N. W. Lekkerkerker, Physica A **202**, 68 (1994).
[6] P. Holmqvist, M. P. Lettinga, J. Buitenhuis, and J. K. G. Dhont, Langmuir **21**, 10976 (2005).
[7] M. J. Stevens and M. O. Robbins, Phys. Rev. E **48**, 3778 (1993).
[8] D. E. Smith, H. P. Babcock, and S. Chu, Science **283**, 1724 (1999).
[9] M. D. Haw, W. C. K. Poon, and P. N. Pusey, Phys. Rev. E **57**, 6859 (1998).
[10] B. J. Ackerson and N. A. Clark, Phys. Rev. A **30**, 906 (1984).
[11] J.-F. Berret, D. C. Roux, G. Porte, and P. Lindner, Europhys. Lett. **25**, 521 (1994).
[12] O. Volkova, S. Cutillas, and G. Bossis, Phys. Rev. Lett. **82**, 233 (1999).
[13] M. P. Lettinga, K. O. Kang, P. Holmqvist, A. Imhof, D. Derks, and J. K. G. Dhont, Phys. Rev. E **73**, 011412 (2006).
[14] R. G. Larson, *The Structure and Rheology of Complex Fluids* (Oxford University Press, New York, 1999).
[15] Ch. Münch and J. Kalus, Rev. Sci. Instrum. **70**, 187 (1999).

[16] P. Panine, M. Gradzielski, and T. Narayanan, Rev. Sci. Instrum. **74**, 2451 (2003).
[17] L. Porcar, W. A. Hamilton, P. D. Butler, and G. G. Warr, Rev. Sci. Instrum. **73**, 2345 (2002).
[18] E. Eiser, F. Molino, G. Porte, and O. Diat, Phys. Rev. E **61**, 6759 (2000).
[19] M. Kisilak, H. Anderson, N. S. Babcock, M. R. Stetzer, S. H. J. Idziak, and E. B. Sirota, Rev. Sci. Instrum. **72**, 4305 (2001).
[20] B. J. Ackerson, J. B. Hayter, N. A. Clark, and L. Cotter, J. Chem. Phys. **84**, 2344 (1986).
[21] S. Ashdown, I. Marković, R. H. Ottewill, P. Lindner, R. C. Oberthür, and A. R. Rennie, Langmuir **6**, 303 (1990).
[22] P. Baroni, C. Pujolle-Robic, and L. Noirez, Rev. Sci. Instrum. **72**, 2686 (2001).
[23] D. Beysens, M. Gbadamassi, and L. Boyer, Phys. Rev. Lett. **43**, 1253 (1979).
[24] B. J. Ackerson, J. Rheol. **34**, 553 (1990).
[25] J. W. van Egmond, D. E. Werner, and G. G. Fuller, J. Chem. Phys. **96**, 7742 (1992).
[26] Y. D. Yan and J. K. G. Dhont, Physica A **198**, 78 (1993).
[27] J. Läuger and W. Gronski, Rheol. Acta **34**, 70 (1995).
[28] I. Cohen, T. G. Mason, and D. A. Weitz, Phys. Rev. Lett. **93**, 046001 (2004).
[29] D. Derks, H. Wisman, A. van Blaaderen, and A. Imhof, J. Phys.: Condens. Matter **16**, S3917 (2004).
[30] M. Paques, A. Imhof, A. van Blaaderen, and Y. Nicolas, European Patent number EP1312910.
[31] R. Biehl and T. Palberg, Rev. Sci. Instrum. **75**, 906 (2004).
[32] Y. Nicolas, M. Paques, A. Knaebel, A. Steyer, J. P. Münch, T. B. J. Blijdenstein, and G. A. van Aken, Rev. Sci. Instrum. **74**, 3838 (2003).
[33] V. A. Tolpekin, M. H. G. Duits, D. van den Ende, and J. Mellema, Langmuir **20**, 2614 (2004).
[34] N. Grizzuti and O. Bifulco, Rheol. Acta **36**, 406 (1997).
[35] K. H. de Haas, D. van den Ende, C. Blom, E. G. Altena, G. J. Beukema, and J. Mellema, Rev. Sci. Instrum. **69**, 1391 (1998).
[36] V. Breedveld, D. van den Ende, M. Bosscher, R. J. J. Jongschaap, and J. Mellema, Phys. Rev. E **63**, 021403 (2001).
[37] S. Kim, J. Yu, and C. C. Han, Rev. Sci. Instrum. **67**, 3940 (1996).
[38] M. D. Haw, W. C. K. Poon, P. N. Pusey, P. Hebraud, and F. Lequeux, Phys. Rev. E **58**, 4673 (1998).
[39] S. Guido and M. Simeone, J. Fluid Mech. **357**, 1 (1998).
[40] K. Matsuzaka and T. Hashimoto, Rev. Sci. Instrum. **70**, 2387 (1999).
[41] T. Solomon and M. J. Solomon, J. Chem. Phys. **124**, 134905 (2006).
[42] M. Minsky, Scanning **10**, 128 (1988).
[43] A. van Blaaderen, A. Imhof, W. Hage, and A. Vrij, Langmuir **8**, 1514 (1992).
[44] A. van Blaaderen and P. Wiltzius, Science **270**, 1177 (1995).
[45] A. van Blaaderen, Prog. Colloid Polym. Sci. **104**, 59 (1997).
[46] W. K. Kegel and A. van Blaaderen, Science **287**, 290 (2000).
[47] U. Gasser, E. R. Weeks, A. Schofield, P. N. Pusey, and D. A. Weitz, Science **292**, 258 (2001).
[48] G. I. Taylor, Proc. R. Soc. London, Ser. A **146**, 501 (1934).
[49] W. Stöber, A. Fink, and E. Bohn, J. Colloid Interface Sci. **26**, 62 (1968).
[50] A. van Blaaderen and A. Vrij, Langmuir **8**, 2921 (1992).